Letter

Process of dissociation of NH_3 by electron impact in low-temperature plasma and its isotope effect

Xianwu Jiang [1,*] Yingqi Chen [1,*] Hainan Liu,[2] Chi-Hong Yuen [3,4,†] and Viatcheslav Kokoouline [5,‡]

[1]*Department of Physics, Wuhan University of Technology, Wuhan 430074, People's Republic of China*
[2]*Department of Basic Courses, Naval University of Engineering, Wuhan 430033, People's Republic of China*
[3]*Department of Physics, Kansas State University, Manhattan, Kansas 66506, USA*
[4]*Department of Physics, Kennesaw State University, Marietta, Georgia 30060, USA*
[5]*Department of Physics, University of Central Florida, Orlando, Florida 32816, USA*

(Received 10 April 2024; accepted 17 July 2024; published 12 August 2024)

Understanding the dissociative electron attachment (DEA) in low-temperature ammonia plasma is crucial for many technological applications, in particular, for alternative energy sources. However, theoretical modeling of this process has been challenging due to the complex interplay of electronic motion and multidimensional nuclear dynamics. This Letter presents a theoretical approach to investigate the process, applying it to the breakup of the NH_3 molecule by low-energy electrons. The potential energy surface of the NH_3^- 5.5 eV resonant state is computed to elucidate the mechanism of the dissociative process. The cross section of DEA via the 5.5 eV resonance is then calculated for both NH_3 and ND_3. The positions of the peaks in both cross sections and the ratio between them are in excellent agreement with previous experiments. Our findings suggest that the developed theoretical model accurately describes the DEA process and could serve as a useful tool for providing DEA cross sections for other molecules to model low-temperature plasma.

DOI: 10.1103/PhysRevA.110.L020803

Dissociative electron attachment (DEA) is a process where a low-energy electron is resonantly captured by the molecule to form a temporary negative ion (TNI) that subsequently dissociates into reactive neutral radicals and anions [1]. This phenomenon plays a fundamental role across a broad spectrum of contexts, spanning from natural environments such as the interstellar medium, ionosphere, and biological radiation damage [2,3] to various technological applications such as plasma-assisted etching and combustion [4,5]. A theoretical description of this bond-breaking process poses a significant challenge due to the involvement of nonadiabatic coupling between electronic and nuclear motion. While DEA to diatomic molecules has been well studied, a complete theoretical treatment of the vibrational and dissociative dynamics in full dimensionality for DEA processes of polyatomic molecules remains infeasible computationally [1], except a few triatomic molecules, such as H_2O [6–10], CO_2 [11,12], HCN [13,14], ClCN, and BrCN [15]. Consequently, previous theoretical studies typically assumed the dissociation occurs in a subspace of coordinates [16–20]. Recently, Yuen *et al.* [2] proposed a simplified approach based on the theory of O'Malley [21] and Bardsley [22] to treat the DEA process for small polyatomic molecules. This approach was initially applied to theoretically estimate the absolute DEA cross section of H_2CN to evaluate its significance in the formation of CN^- in the interstellar medium. Subsequently, we extended the approach to calculate the DEA cross section of NO_2 [23] but found significant deviations between their results and the experimental results reported by Rangwala *et al.* [24]. Recently, an experiment conducted by Xie *et al.* [25] showed that the measured ratio between the two primary peaks of the DEA cross section closely matched the theoretical predictions [23]. Clearly, further validation of our theoretical approach is desirable.

In this Letter, we apply our DEA theory to the case of NH_3, an ideal hydrogen and energy carrier [26]. As a green fuel, NH_3 has attracted significant attention in the global energy development strategies and has found applications in power plants, as well as combustion engines for vehicles, ships, and spacecraft [27,28]. However, the commercial adoption of NH_3 faces three major limitations: high heat of ignition, flame stability, and NO_x emission. Low-temperature plasma-assisted technology has been demonstrated to effectively address these challenges [29]. As DEA drives the chemistry of the plasma, investigating this process is crucial for understanding the mechanisms of combustion. Consequently, the cross section serves as a vital ingredient in plasma modeling.

Over the years, the DEA process of NH_3 has been extensively studied [16,30–37]. Two resonant peaks are observed around 5.5 and 10.5 eV in the DEA cross sections [30–34]. The 10.5 eV TNI with symmetry ^2E contributes to the formation of $NH_2^*(^2A_1) + H^-(^1S)$ and $NH^-(^2\Pi) + 2H(^2S)$, while the product $NH_2^-(^1A_1) + H(^2S)$ remains a puzzle [16,36]. The lower TNI with symmetry $^2A_1$ is directly associated with the dissociation channel $NH_2(^2B_1) + H^-(^1S)$ and indirectly with the $NH_2^-(^1A_1) + H(^2S)$ channel through nonadiabatic charge transfer at a large nuclear distance [16]. So far, the accuracy of the absolute cross-section measurement for NH_3 DEA remains unclear, as data from a more recent study by Rawat *et al.* [35] differ by 50% from earlier experimental studies by Sharp and Dowell [30] and Compton *et al.* [31].

*These authors contributed equally to this work.
†Contact author: cyuen2@kennesaw.edu
‡Contact author: slavako@ucf.edu

However, the isotope effect determined by the ratio between the DEA cross section of NH_3 and ND_3 is surprisingly consistent.

In contrast to extensive experimental investigations, there has been no theoretical study on the DEA of NH_3 except the computation of potential energy surfaces (PESs) of the NH_3^- TNI states by Rescigno *et al.* [16]. We therefore undertake the theoretical investigation on the DEA process of NH_3 through the 5.5 eV resonance using a method similar to the one by Refs. [2,23].

The equilibrium geometry of NH_3 is pyramidal of the C_{3v} point group. The electronic configuration of the ground state $^1A_1$ is $1a_1^2 2a_1^2 1e^4 3a_1^2$. The MOLPRO package [38] is used to determine the molecular electronic structure and vibrational frequencies. For the purpose of describing molecular vibration, the C_s symmetry was used in this study for electronic structure calculations. Hartree-Fock (HF) orbitals obtained with correlation-consistent polarized valence triple (cc-pVTZ) basis set are used in the complete active space (CAS) self-consistent field (CASSCF) method to optimize the equilibrium geometry of NH_3. Four electrons are kept frozen in the core orbitals and the outer six valence electrons are distributed freely in the CAS of $3a'$, $1a''$, $4a'$, $5a'$, $2a''$, and $6a'$ using the C_s symmetry notations. Frequencies for six vibrational modes, N-H wagging (ν_1), doubly degenerate H-N-H scissoring (ν_2), N-H symmetric stretch (ν_3), and doubly degenerate N-H asymmetric stretch (ν_4), are computed and found to agree with the experimental values. More calculation details could be found in Ref. [39].

To find energies and widths of the resonance as a function of geometry, we have performed electron-scattering calculations using the UKRMOL+ code with the help of the QUANTEMOL-EC interface [40–42]. The CASSCF orbitals from MOLPRO calculation are used by the CAS configuration interaction (CAS-CI) method to construct the target's electronic states. Seventeen states below 15 eV are included in the closed-coupling scattering model. The R matrix is established on the R-sphere boundary of 12 bohrs and then propagated to asymptotic distances to yield the reaction matrix (K matrix). The eigenphase sum for partial waves with $l \leqslant 4$ is obtained through the K matrix. Then, the position Δ and width Γ of the TNI resonances at each nuclear geometry are obtained by fitting the eigenphase sum in the Breit-Wigner form. Two resonances of $^2A_1$ and ^2E symmetries peak around 5.5 and 10.5 eV at equilibrium geometry could be respectively formed by capturing the incident electron into the $4a_1$ Rydberg orbital by the excited NH_3 where one of the $3a_1$ or $1e$ valence electrons is promoted to $4a_1$. In the scattering model the same CAS as in the MOLPRO calculation is employed. Resonance energies are found to be 5.51 and 10.91 eV with widths of 0.0097 and 0.0277 eV. They agree well with the experimental values as seen from Table 4 in Ref. [39], indicating the accuracy of the scattering model used in this study.

Figure 1 shows the computed resonance energies Δ of the 5.5 eV TNI state $^2A_1$ as a function to the normal coordinate q in the four vibrational modes. The resonance energy is nearly constant along displacements in H-N-H scissoring and N-H asymmetric stretch modes, which means that the PES of the resonant state along q_2 and q_4 near the equilibrium is not repulsive state (following the PES of the neutral molecule).

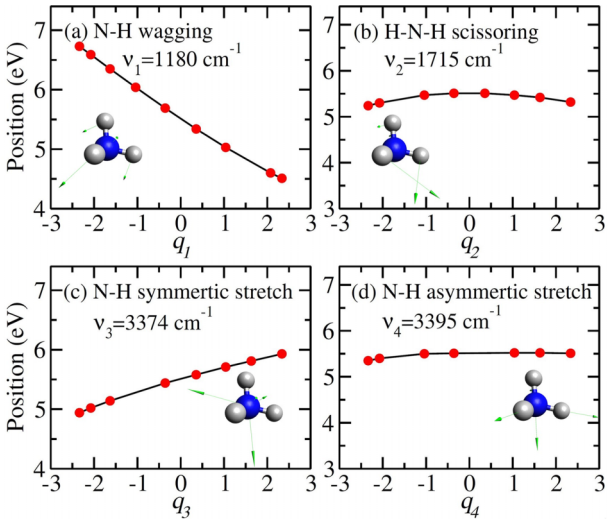

FIG. 1. Variation of the resonance energies Δ with respect to the ground state energy of NH_3 as a function of normal coordinates: (a) q_1 of N-H wagging with $\nu_1 = 1180\ \mathrm{cm}^{-1}$, (b) q_2 of H-N-H scissoring with $\nu_1 = 1715\ \mathrm{cm}^{-1}$, (c) q_3 of N-H symmetric stretch with $\nu_1 = 3374\ \mathrm{cm}^{-1}$, (d) q_4 of N-H asymmetric stretch with $\nu_4 = 3395\ \mathrm{cm}^{-1}$. The insets display the four normal modes of NH_3.

However, variation of the resonance energy is strong along the N-H wagging and N-H symmetric stretch modes, indicating that the coordinates q_1 and q_3 participate in the dissociation process. The two nuclear vibrational motions will couple together in the dissociation of the 5.5 eV NH_3^- TNI after the electron attaches to NH_3: The anion system will slide down towards to dissociation geometries along the path of the steepest descent of the anionic PES.

As in our earlier study of H_2CN [2], the capture coordinate is obtained using an orthogonal matrix transforming (q_1, q_3) to (s_1, s_2):

$$\begin{pmatrix} \alpha & \beta \\ -\beta & \alpha \end{pmatrix} \begin{pmatrix} q_1 \\ q_3 \end{pmatrix} = \begin{pmatrix} s_1 \\ s_2 \end{pmatrix}. \tag{1}$$

If s_1 is the steepest descent coordinate, then

$$\frac{\partial \Delta}{\partial s_1} = \alpha \frac{\partial \Delta}{\partial q_1} + \beta \frac{\partial \Delta}{\partial q_3}, \tag{2}$$

where α is

$$\alpha = \frac{|\partial \Delta / \partial q_1|}{\sqrt{(\partial \Delta / \partial q_1)^2 + (\partial \Delta / \partial q_3)^2}} \tag{3}$$

and $\beta = \sqrt{1 - \alpha^2}$. Scattering calculations performed for different s_1 produce resonance energies $\Delta(s_1)$ and widths as a function s_1. The anion PES denoted by $U_d(s_1)$ is obtained by

$$U_d(s_1) = \tfrac{1}{2} \hbar \tilde{\nu_1}^2 + \Delta(s_1), \tag{4}$$

with

$$\tilde{\nu_1} = \alpha^2 \nu_1 + \beta^2 \nu_3. \tag{5}$$

Figure 2 displays the computed resonance energies $\Delta(s_1)$ and the potential energy $U_n(s_1)$ of the neutral NH_3. The red solid

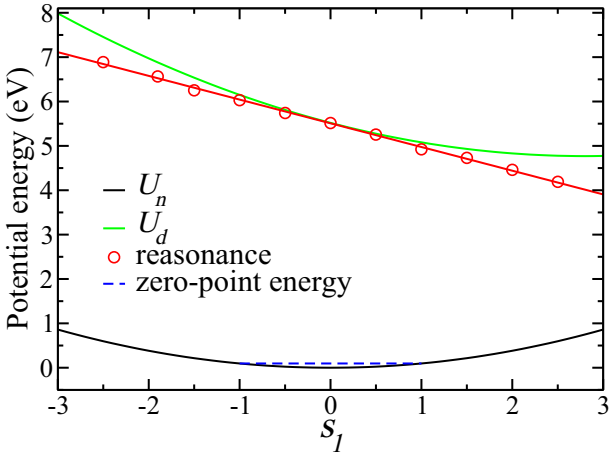

FIG. 2. Potential energy along the steepest-descent coordinate s_1. $U_n(s_1)$ (black solid line) is the PES of the neutral NH_3. Resonance energies $\Delta(s_1)$ (red line) are obtained by a linear fit using the data shown by red circles computed at discrete values of s_1. $U_d(s_1)$ is the anionic PES of NH_3^- obtained by adding $U_d(s_1)$ and Δ. Vibrational zero-point energy $\frac{1}{2}\hbar\tilde{\nu}_1$ is shown by the blue dashed horizontal line.

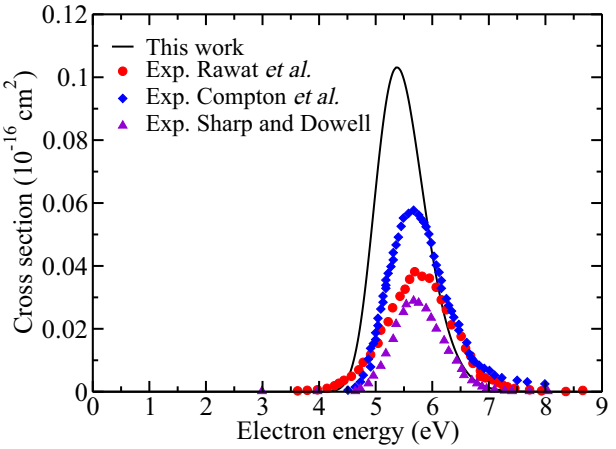

FIG. 3. DEA cross section obtained in this work (black solid curve) and observed experimentally by Sharp and Dowell [30] (green dotted curve), Compton *et al.* [31] (blue dotted curve), and Rawat *et al.* [35] (red dotted curve). The computed DEA cross section is convoluted with the uncertainty of 0.5 eV.

line represents the linear fit of $\Delta(s_1)$ by

$$\Delta(s_1) = \Delta(s_1 = 0) + \frac{d\Delta(s_1)}{ds_1} s_1, \tag{6}$$

with which the potential energy $U_n(s_1)$ of 5.5 eV NH_3^- TNI is computed by Eq. (4). The figure demonstrates that after electron attachment, the anion complex will slide down to dissociation along $U_d(s_1)$ within the Franck-Condon region.

According to the WKB approach by O'Malley [21] and Bardsley [22], the capture cross section is given in atomic units

$$\sigma_{\rm cap}(\varepsilon) = g\frac{\pi^2}{\varepsilon}\frac{\Gamma_d(s_\varepsilon)}{|U_d'(s_E)|}|\eta_{\tilde{\nu}_1}(s_E)|^2, \tag{7}$$

where ε and E are the electron scattering energy and the total energy of the scattering system. The Franck-Condon point s_ε and the classical turning point s_E are located by solving $\Delta(s_\varepsilon) = \varepsilon$ and $U_d(s_E) = E$, respectively. $\eta_{\tilde{\nu}_1}$ is the ground vibrational state along the capture coordinate s_1. The factor g is the ratio of spin multiplicities in the final and initial states, which equals to 1 in the present case because the final and initial spin states of the $NH_3 + e^-$ system are doublets. Finally, the DEA cross section accounting for the survival probability $P_s(\varepsilon)$ [23] is computed as

$$\sigma_{\rm DEA}(\varepsilon) = \sigma_{\rm cap}(\varepsilon)P_s(\varepsilon). \tag{8}$$

The survival probability $P_s(\varepsilon)$ specifies the dissociation probability. It is determined by using the WKB approximation [23]

$$P_s = \exp\left(-\frac{1}{\hbar}\int_{t_E}^{t_s}\Gamma(s_1)dt\right) = \exp\left(-\frac{1}{\hbar}\int_{s_E}^{s_\varepsilon}\frac{\tilde{\Gamma}(s_1)}{v(s_1)}ds_1\right), \tag{9}$$

where $\tilde{\Gamma} = \Gamma/\hbar\tilde{\nu}$ is the dimensionless resonance width. $v(s_1) = \sqrt{2[(E - U_d(s_1)/\hbar\tilde{\nu}]}$ is the dimensionless velocity. The integration is performed in the region between the classical turning point s_E and the Franck-Condon point s_ε.

The DEA cross section obtained with Eq. (8) is convoluted with the uncertainty of 0.5 eV [35] to compare with the experimental measurements by Rawat *et al.* [35], Compton *et al.* [31], and Sharp and Dowell [30]. The comparison is shown in Fig. 3. The main features of the theoretical and experimental cross sections are listed and compared in Table I.

The peak value of the theoretical cross section is higher than in the experiments: almost twice higher than that in Compton *et al.* [31]. While we are quite confident in the accuracy of the *ab initio* description of the electron attachment and initial dynamics of NH_3^- towards to dissociation, the disagreement in the magnitude of the cross section with the experiment suggests that in the theoretical model there could be a potential barrier along the dissociation path, which reduces the DEA flux. We have therefore computed the PES of the 5.5 eV resonance state in a large domain of geometries. The 5.5 eV resonance with an electronic configuration of $1a_1^2 2a_1^2 1e^3 3a_1^2 4a_1^2$ is made up of a $4a_1$ Rydberg electron bound to the excited state a^3A_1 of NH_3. It is thus a Feshbach-type resonance [16,32,33]. We use the MOLPRO package [38]

TABLE I. Positions (eV) and magnitudes (10^{-18} cm^{-2}) of maximum of the DEA cross sections for NH_3 and ND_3.

	This work		Rawat *et al.* [35]		Compton *et al.* [31]		Sharp and Dowell [30]	
Isotope molecule	Position	Cross section	Position	Cross section	Position	Cross section	Position	Cross section
NH_3	5.4	10.3	5.7	3.9	5.7	5.74	5.65	2.9
ND_3	5.7	9.36	–	–	5.86	5.36	5.65	2.6

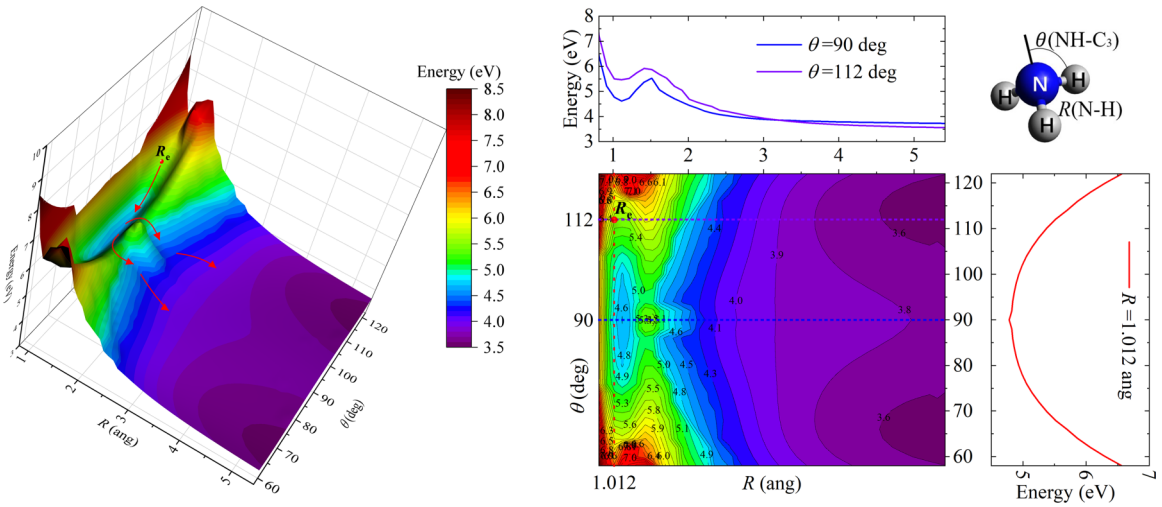

FIG. 4. PES of the 5.5 eV NH_3^- TNI state $^2A_1$ as a function of the N-H nuclear distance R(N-H) and the angle θ(NH-C_3) between the NH bond and C_3 axis. The surface is shown in the left panel. The arrows indicate the DEA flux on the surface starting from the equilibrium geometry R_e of the neutral NH_3 marked by a red dot where the incident electron is captured. The right panel shows the PES by isosurfaces. Horizontal lines representing the PES of the $^2A_1$ state obtained with θ fixed at 90° (in blue) and 112° (in violet) and R(N-H) stretched, are given on the top. Red vertical lines is the PES computed fixing R(N-H) at 1.012 Å and varying θ.

performing CASSCF calculations using the diffuse basis set augmented correlation-consistent polarized valence triple zeta (aug-cc-pVTZ) with the f-type functions on N and d-type functions on H excluded and a CAS closing one core orbital and distributing freely the outer nine electrons in 11 active orbitals. Potential energies are obtained as functions of the N-H nuclear distance R(N-H) and the angle θ(NH-C_3) between the NH bond and the C_3 axis. The PES of the resonance with the energy origin at the NH_3 equilibrium R_e is displayed in Fig. 4. A broad valley on the surface centered at $\theta = 90°$ indicates a planar equilibrium geometry of the $^2A_1$ resonance state. It is similar in shape to its parent state a^3A_1 and the "grandparent" NH_3^+ cation. The PES obtained, if R(N-H) is fixed at equilibrium, is thus parabolic as θ varies. Predissociation of the well-defined vibrational levels of the N-H wagging mode within the quasibound state explains the progression of narrow peaks in the DEA cross sections found by Tronc *et al.* [33] and Stricklett and Burrow [32]. A bump is observed as R stretches at every individual θ, e.g., 90° and the equilibrium value of about 112°. Especially, a bump is around at $\theta = 90°$, generating a saddle structure with increased R. The reason that experimental angular distributions of the anionic fragments H^- and NH_2^- presenting minimum at 90° is immediately apparent. As pointed out by Rescigno *et al.* [16], the 5.5 eV NH_3^- TNI will dissociate with θ flattened and R stretched simultaneously, i.e., dissociation flux indicated by the arrows on the surface is free from an energy barrier.

The significant discrepancy between the computed and experimental DEA cross sections, as well as the disagreement between three different experiments, urge us a further consider the process, considering the isotopolog molecule ND_3, for which experimental data also exist. Using the same approach, we computed the DEA cross section for ND_3. The results obtained are briefly summarized and compared with the experiments in Table I. Similar to NH_3, the theoretical cross section for ND_3 is larger than in the experiments [31]. However, the ratios of the NH_3 and ND_3 cross sections, obtained in the experiment and theory, agree surprisingly very well: Figure 5 compares the theoretical and experimental [30,31] cross sections normalized to NH_3 peak values. Given that the experimental DEA cross sections still disagree with each other and, therefore, cannot be étalons to benchmark the theory, the fact that the NH_3/ND_3 ratios agree well justifies the present theoretical approach.

To conclude, we have studied DEA to the NH_3 molecule through the 5.5 eV resonance. The cross sections obtained for NH_3 and ND_3 isotopologs are larger by factors 2–4 compared to the available experimental data, while the experimental cross sections measured by three groups differ from each other by about a factor of 2. On the other hand, an excellent

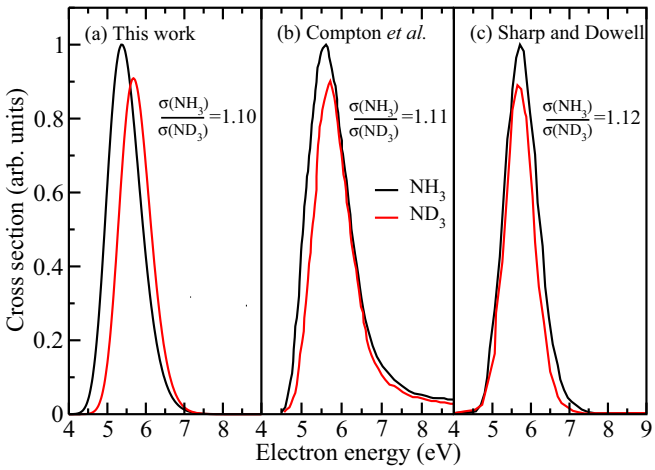

FIG. 5. Comparison of the DEA cross sections for the NH_3 and ND_3 isotopologs from the present study [(a)], and two experiments [(b) [31] and (c) [30]]. The NH_3 and ND_3 cross sections in each panel are scaled by a factor such that the NH_3 cross section is 1 at its maximum. The ratio $\sigma_{NH_3}/\sigma_{ND_3}$ of the peak values of the cross sections are indicated in the panels.

agreement of the present theory with two experiments was found for the ratio of cross sections for the two isotopologs. Given that the experiments disagree with each other in calibration of the absolute cross section, the excellent agreement for the ratio with the two experiments validates the present approach and suggests also that the absolute cross sections obtained in this study are also accurate. In addition, the PES of the 5.5 eV NH_3^- resonance was studied and computed as a function of the N-H distance and the angle of between the N-H bond and the molecular axis, i.e., for C_{3v} geometries. The determination of the PES has been informative in revealing the DEA mechanism. The PES can also help modeling the structure of overlapping peaks produced by N-H wagging-mode vibration and shed light on the branching ratios in the dissociation products. Such a study will be performed in a future.

This work acknowledges the support from Natural Science Foundation of Hubei Province (Grant No. 20221j0064), National Natural Science Foundation of China (Grants No. 12204544 and No. 12304277), and the National Science Foundation Grant No. PHY-2110279.

[1] I. I. Fabrikant, S. Eden, N. J. Mason, and J. Fedor, Adv. At., Mol., Opt. Phys. **66**, 545 (2017).
[2] C. H. Yuen, N. Douguet, S. Fonseca dos Santos, A. E. Orel, and V. Kokoouline, Phys. Rev. A **99**, 032701 (2019).
[3] B. Boudaïffa, P. Cloutier, D. Hunting, M. A. Huels, and L. Sanche, Science **287**, 1658 (2000).
[4] L. G. Christophorou and J. K. Olthoff, Int. J. Mass Spectrom. **205**, 27 (2001).
[5] Y. Ju and W. Sun, Prog. Energy Combust. Sci. **48**, 21 (2015).
[6] D. J. Haxton, Z. Zhang, H.-D. Meyer, T. N. Rescigno, and C. W. McCurdy, Phys. Rev. A **69**, 062714 (2004).
[7] D. J. Haxton, T. N. Rescigno, and C. W. McCurdy, Phys. Rev. A **75**, 012711 (2007).
[8] D. J. Haxton, C. W. McCurdy, and T. N. Rescigno, Phys. Rev. A **75**, 012710 (2007).
[9] D. J. Haxton, T. N. Rescigno, and C. W. McCurdy, Phys. Rev. A **78**, 040702(R) (2008).
[10] H. Adaniya, B. Rudek, T. Osipov, D. J. Haxton, T. Weber, T. N. Rescigno, C. W. McCurdy, and A. Belkacem, Phys. Rev. Lett. **103**, 233201 (2009).
[11] D. Slaughter, H. Adaniya, T. Rescigno, D. Haxton, A. Orel, C. McCurdy, and A. Belkacem, J. Phys. B: At., Mol. Opt. Phys. **44**, 205203 (2011).
[12] A. Moradmand, D. S. Slaughter, D. J. Haxton, T. N. Rescigno, C. W. McCurdy, T. Weber, S. Matsika, A. L. Landers, A. Belkacem, and M. Fogle, Phys. Rev. A **88**, 032703 (2013).
[13] S. T. Chourou and A. E. Orel, Phys. Rev. A **80**, 032709 (2009).
[14] S. T. Chourou and A. E. Orel, Phys. Rev. A **83**, 032709 (2011).
[15] J. Royal and A. Orel, J. Chem. Phys. **125**, 214307 (2006).
[16] T. N. Rescigno, C. S. Trevisan, A. E. Orel, D. S. Slaughter, H. Adaniya, A. Belkacem, M. Weyland, A. Dorn, and C. W. McCurdy, Phys. Rev. A **93**, 052704 (2016).
[17] H. Li, X.-F. Gao, X. Meng, and S. X. Tian, Phys. Rev. A **99**, 032703 (2019).
[18] M. Zawadzki, M. Čížek, K. Houfek, R. Čurík, M. Ferus, S. Civiš, J. Kočišek, and J. Fedor, Phys. Rev. Lett. **121**, 143402 (2018).
[19] H. B. Ambalampitiya and I. I. Fabrikant, Phys. Rev. A **102**, 022802 (2020).
[20] J. Trnka, K. Houfek, and M. Čížek, Phys. Rev. A **109**, 012803 (2024).
[21] T. F. O'Malley, Phys. Rev. **150**, 14 (1966).
[22] J. N. Bardsley, J. Phys. B: At. Mol. Phys. **1**, 349 (1968).
[23] H. Liu, X. Jiang, C.-H. Yuen, V. Kokoouline, and M. Ayouz, J. Phys. B: At., Mol. Opt. Phys. **54**, 185201 (2021).
[24] S. A. Rangwala, E. Krishnakumar, and S. V. K. Kumar, Phys. Rev. A **68**, 052710 (2003).
[25] J. Xie, M. Fan, and S. X. Tian, J. Phys. Chem. Lett. **14**, 598 (2023).
[26] J. Guo and P. Chen, Chem **3**, 709 (2017).
[27] A. Valera-Medina, F. Amer-Hatem, A. K. Azad, I. C. Dedoussi, M. de Joannon, R. X. Fernandes, P. Glarborg, H. Hashemi, X. He, S. Mashruk, J. McGowan, C. Mounaim-Rouselle, A. Ortiz-Prado, A. Ortiz-Valera, I. Rossetti, B. Shu, M. Yehia, H. Xiao, and M. Costa, Energy Fuels **35**, 6964 (2021).
[28] B. E. Snyder, A. B. Turkiewicz, H. Furukawa, M. V. Paley, E. O. Velasquez, M. N. Dods, and J. R. Long, Nature (London) **613**, 287 (2023).
[29] J. Choe, W. Sun, T. Ombrello, and C. Carter, Combust. Flame **228**, 430 (2021).
[30] T. Sharp and J. Dowell, J. Chem. Phys. **50**, 3024 (1969).
[31] R. Compton, J. Stockdale, and P. Reinhardt, Phys. Rev. **180**, 111 (1969).
[32] K. Stricklett and P. Burrow, J. Phys. B: At. Mol. Phys. **19**, 4241 (1986).
[33] M. Tronc, R. Azria, and M. B. Arfa, J. Phys. B: At., Mol. Opt. Phys. **21**, 2497 (1988).
[34] T. Yalcin and S. Suzer, J. Mol. Struct. **266**, 353 (1992).
[35] P. Rawat, V. S. Prabhudesai, M. Rahman, N. B. Ram, and E. Krishnakumar, Int. J. Mass Spectrom. **277**, 96 (2008).
[36] N. B. Ram and E. Krishnakumar, J. Chem. Phys. **136**, 164308 (2012).
[37] D. Chakraborty, A. Giri, and D. Nandi, Phys. Chem. Chem. Phys. **21**, 21908 (2019).
[38] H.-J. Werner, P. J. Knowles, F. R. Manby, J. A. Black, K. Doll, A. Heßelmann, D. Kats, A. Köhn, T. Korona, D. A. Kreplin, Q. Ma, I. Miller, T. F. Miller, III, A. Mitrushchenkov, K. A. Peterson, I. Polyak, G. Rauhut, and M. Sibaev, J. Chem. Phys. **152**, 144107 (2020).
[39] Y. Chen, X. Jiang, L. Yao, W. Jiang, H. Liu, and Y. Zhang, Plasma Sources Sci. Technol. **32**, 045017 (2023).
[40] J. Tennyson, Phys. Rep. **491**, 29 (2010).
[41] B. Cooper, M. Tudorovskaya, S. Mohr, A. O'Hare, M. Hanicinec, A. Dzarasova, J. D. Gorfinkiel, J. Benda, Z. Mašín, A. F. Al-Refaie, P. J. Knowles, and J. Tennyson, Atoms **7**, 97 (2019).
[42] Z. Mašín, J. Benda, J. D. Gorfinkiel, A. G. Harvey, and J. Tennyson, Comput. Phys. Commun. **249**, 107092 (2020).